Supporting Information for

Structure-Redox-Relaxivity Relationships for Redox Responsive Manganese-Based Magnetic Resonance Imaging Probes

Eric M. Gale,[‡] Shreya Mukherjee,[‡] Cynthia Liu, Galen Loving, Peter Caravan*

[‡]Authors contributed equally to this manuscript

Athinoula, A. Martinos Center for Biomedical Imaging, Department of Radiology, Massachusetts General Hospital, Harvard Medical School, 149 Thirteenth Street, Charlestown, Massachusetts 02129

Table of Contents

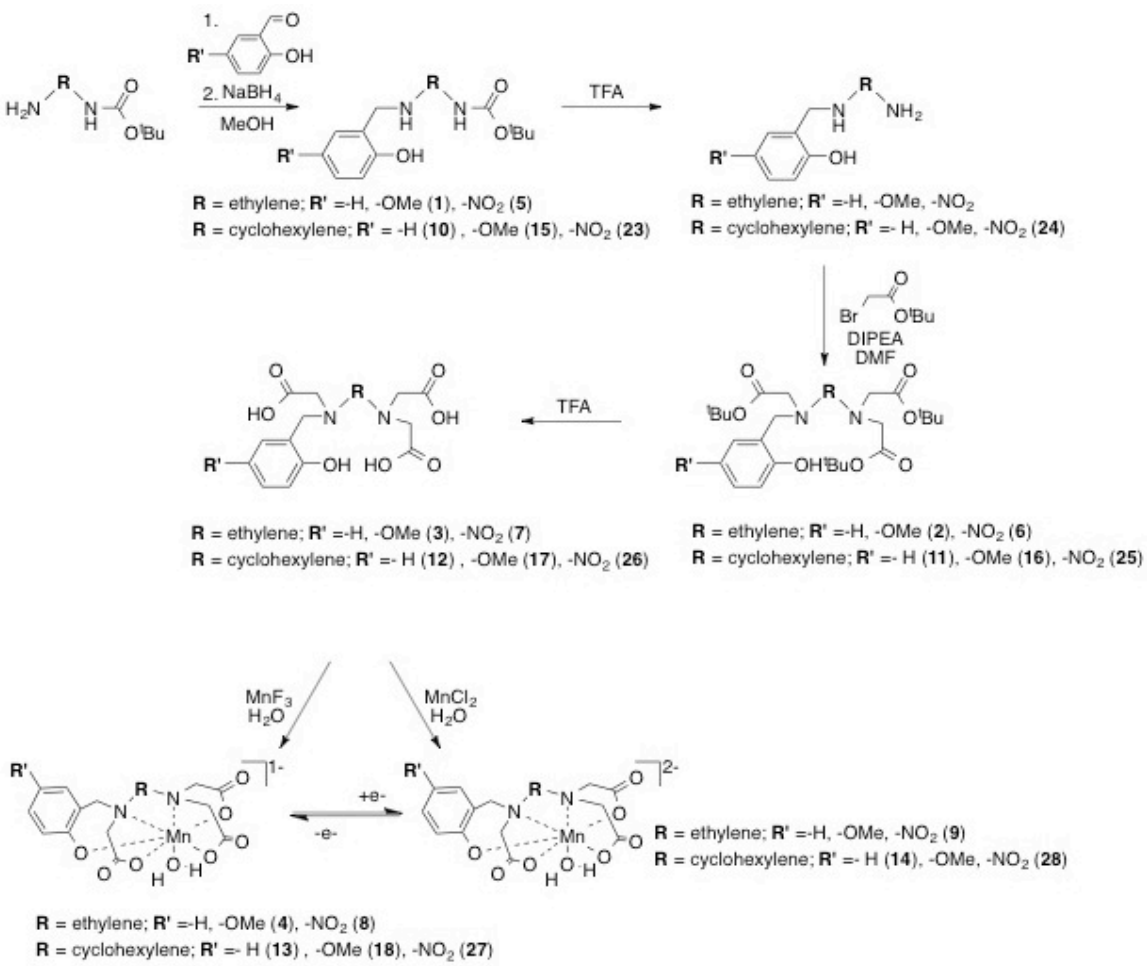

Scheme S1. Synthesis of ligands, Mn(II) complexes, and Mn(III) complexes considered in this study.

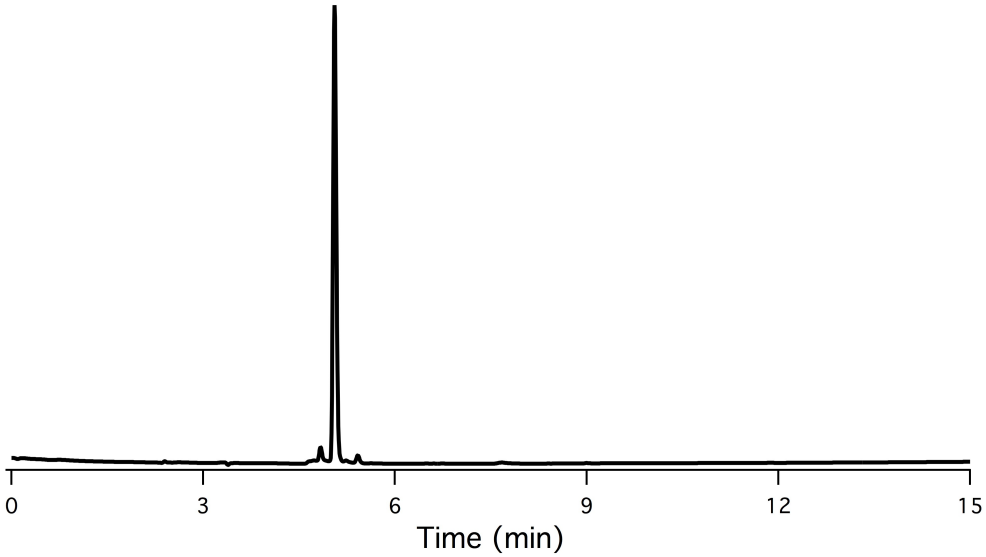

Figure S1. LC of $[Mn(HBET\text{-}OMe)]^{2-}$ detected at 220 nm; m/z^{+} = 424.1 eluted with this peak.

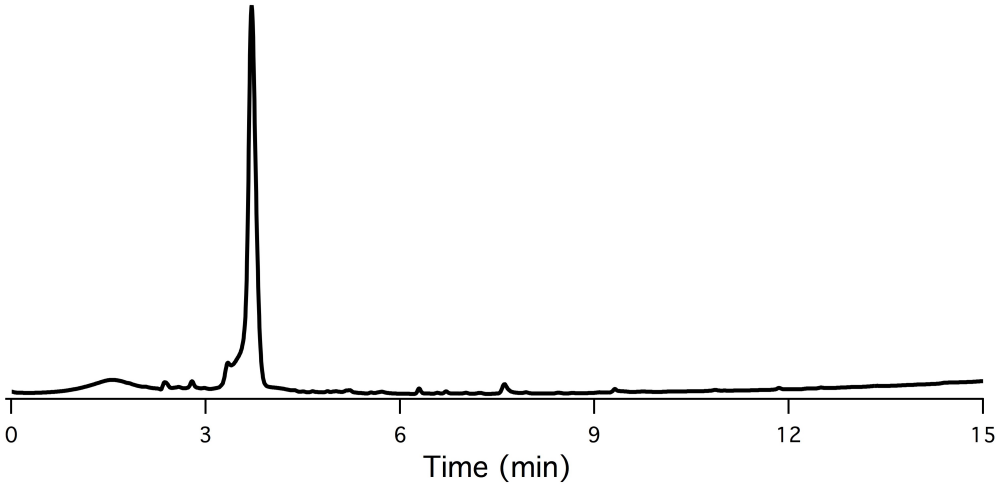

Figure S2. LC of $[Mn(HBET\text{-}NO_2)]^{2-}$ detected at 254 nm; m/z^{+} = 439.0 eluted with this peak.

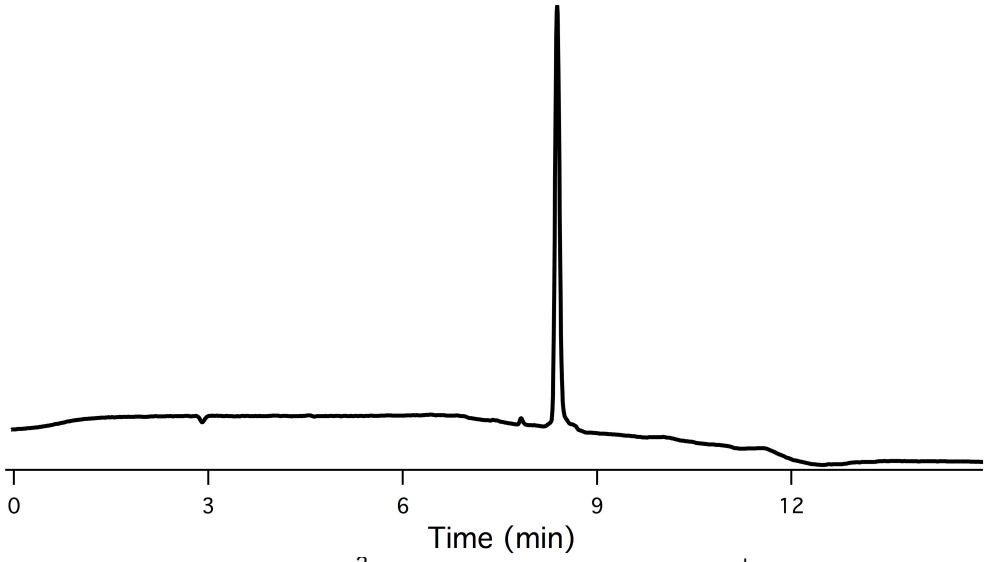

Figure S3. LC of $[Mn(CyHBET)]^{2-}$ detected at 220 nm; m/z^{+} = 448.3 eluted with this peak.

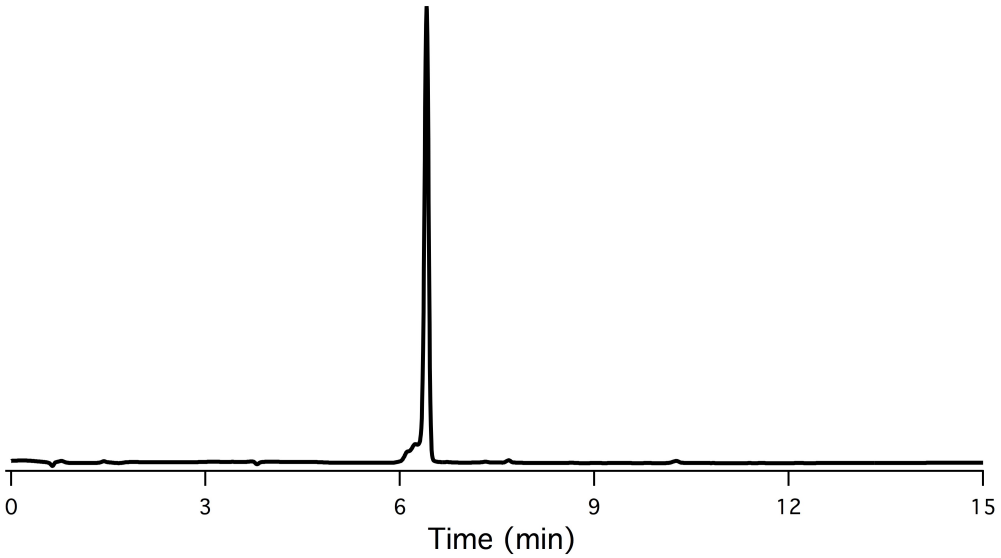

Figure S4. LC of $[Mn(CyHBET\text{-}OMe)]^{2-}$ detected at 220 nm; m/z^{+} = 478.1 eluted with this peak.

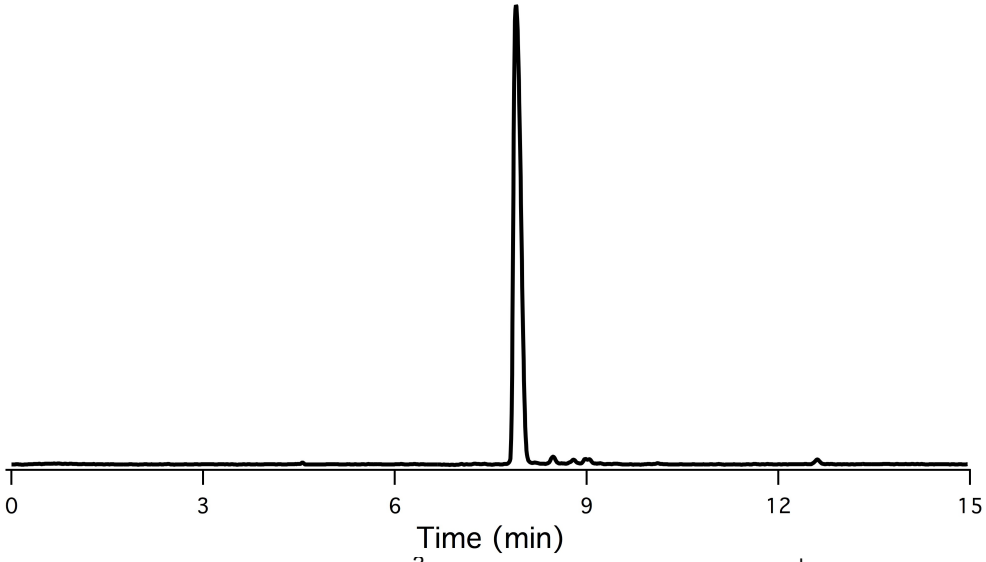

Figure S5. LC of $[Mn(CyHBET\text{-}NO_2)]^{2-}$ detected at 220 nm; m/z^+ = 494.1 eluted with this peak.

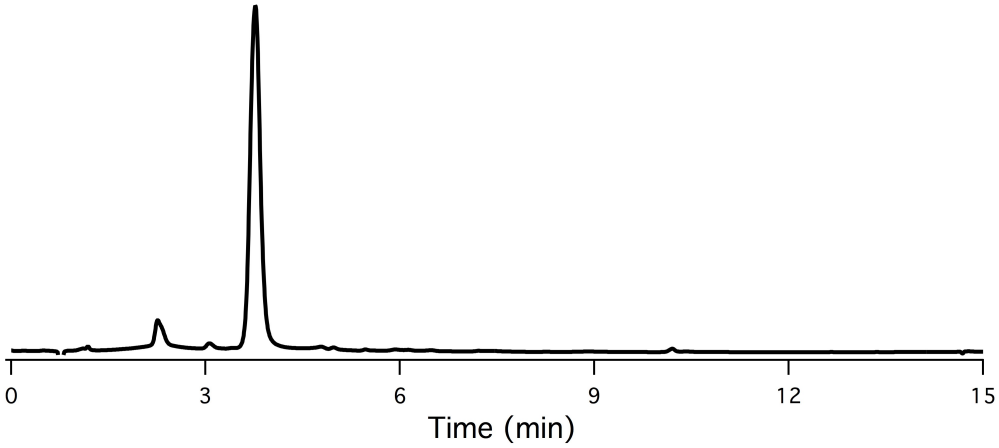

Figure S6. LC of $[Mn(HBET\text{-}NO_2)]^-$ detected at 280 nm; m/z^+ = 438.0 eluted with this peak.

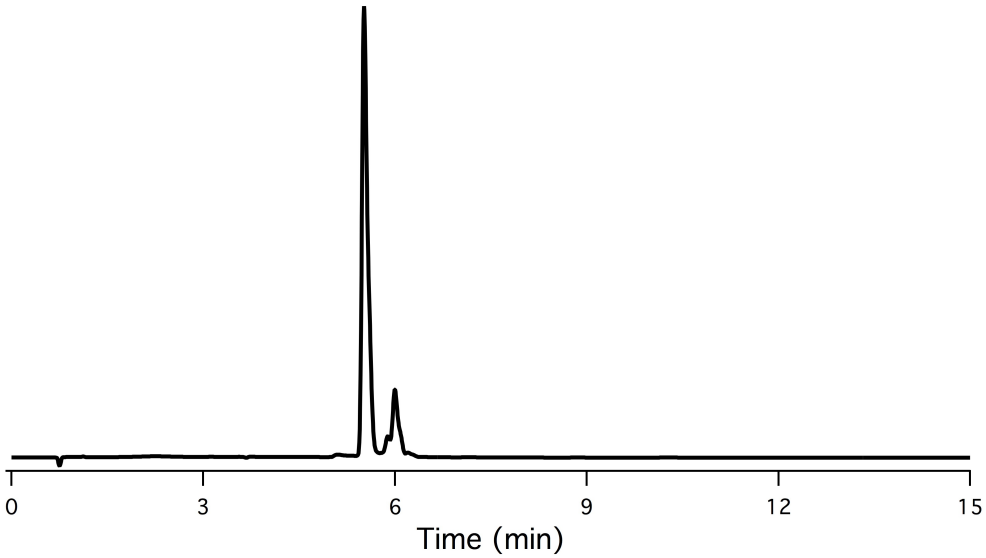

Figure S7. LC of $[Mn(CyHBET)]^-$ detected at 254 nm showing both diastereomeric forms of this complex; m/z^+ = 447.4 eluted with these peaks.

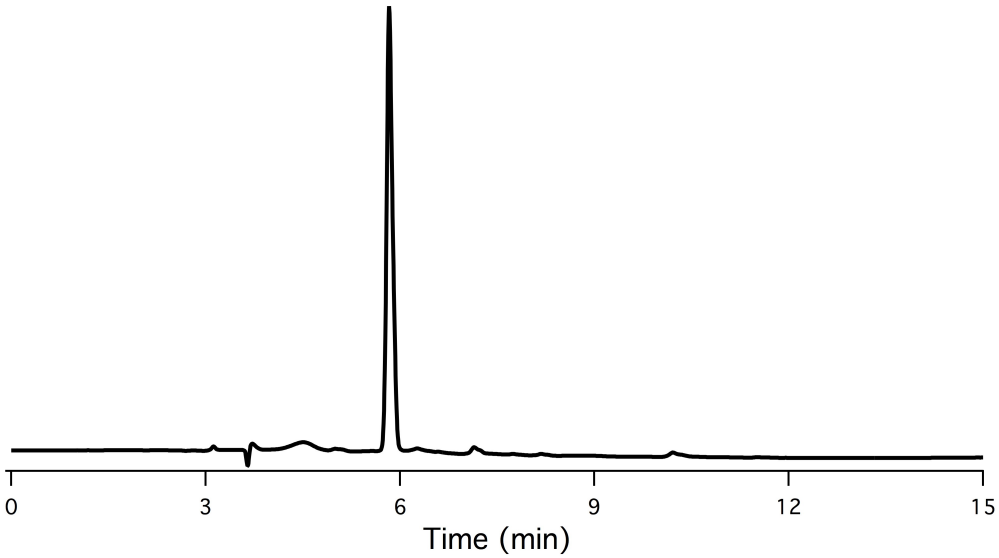

Figure S8. LC of one unique diastereomer of $[Mn(CyHBET\text{-}NO_2)]^-$ detected at 254 nm; m/z^+ = 493.1 eluted with this peak.

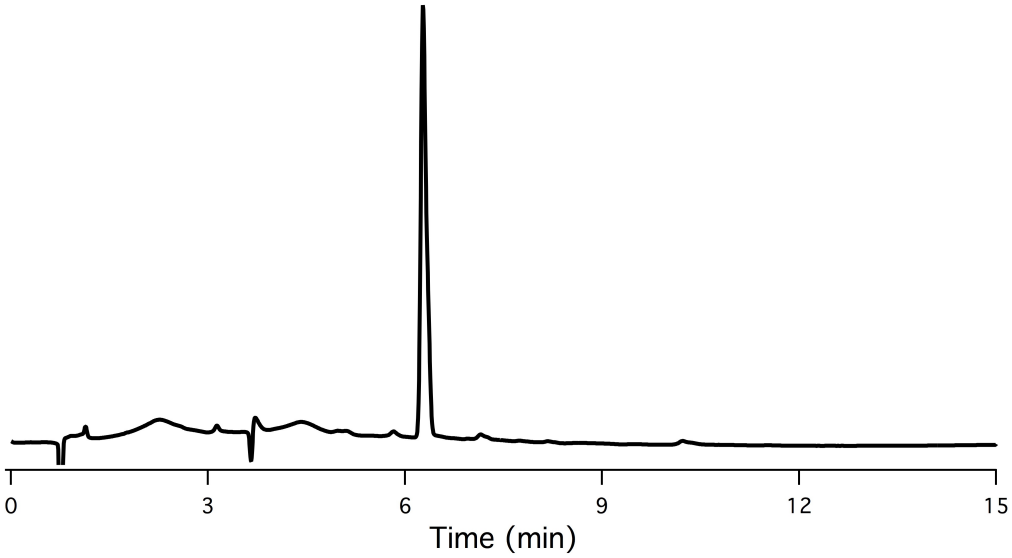

Figure S9. LC of the other unique diastereomer of $[Mn(CyHBET\text{-}NO_2)]^-$ detected at 254 nm; m/z^+ = 493.1 eluted with this peak.

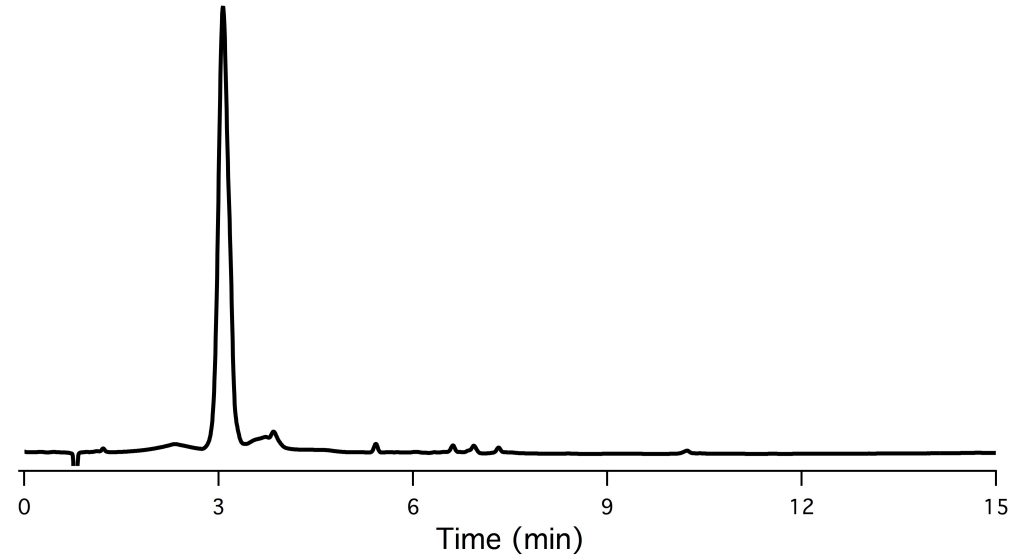

Figure S10. LC of $[Zn(HBET)]^{2-}$ detected at 280 nm; m/z^+ = 403.1 eluted with this peak.

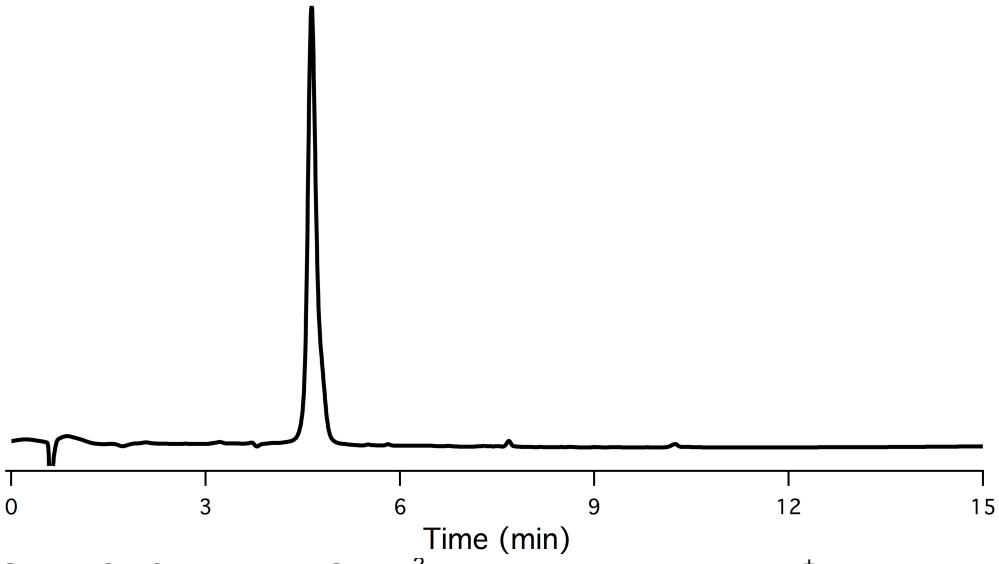

Figure S11. LC of $[Zn(HBET\text{-}OMe)]^{2-}$ detected at 280 nm; m/z^{+} = 431.1 eluted with this peak.

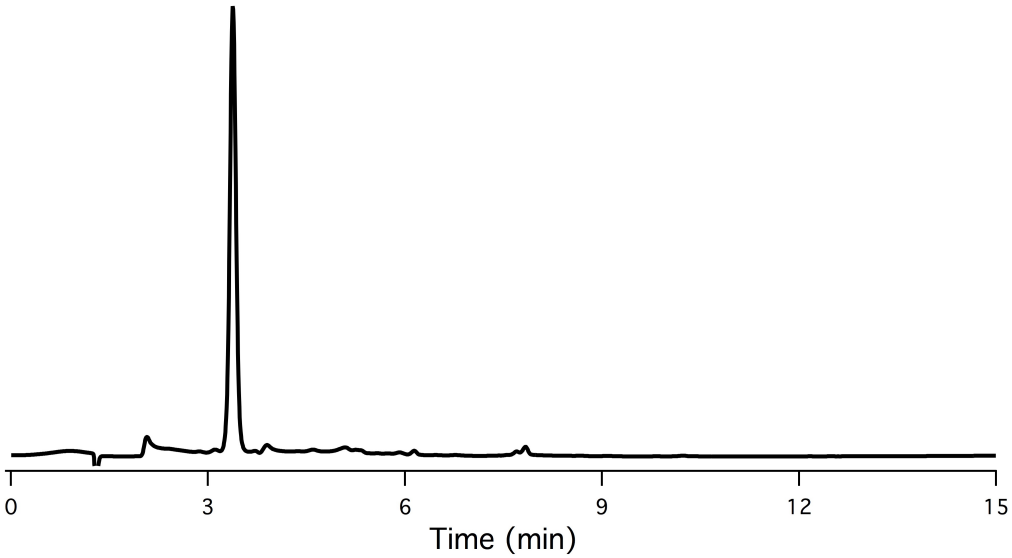

Figure S12. LC of $[Zn(HBET\text{-}NO_2)]^{2-}$ detected at 280 nm; m/z^{+} = 448.0 eluted with this peak.

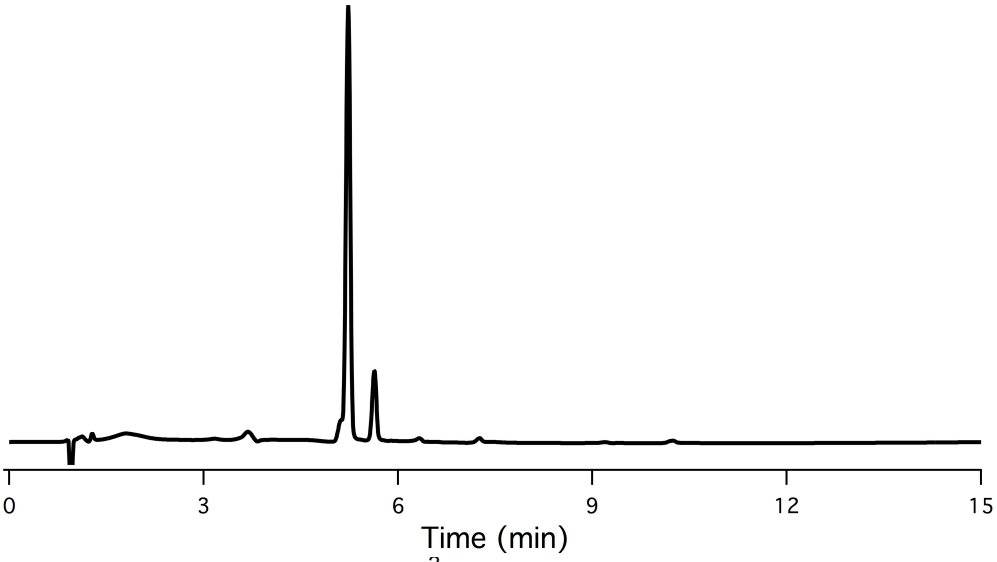

Figure S13. LC of $[Zn(CyHBET)]^{2-}$ detected at 280 nm showing both diastereomeric forms of this complex; m/z^{+} = 457.1 eluted with these peaks.

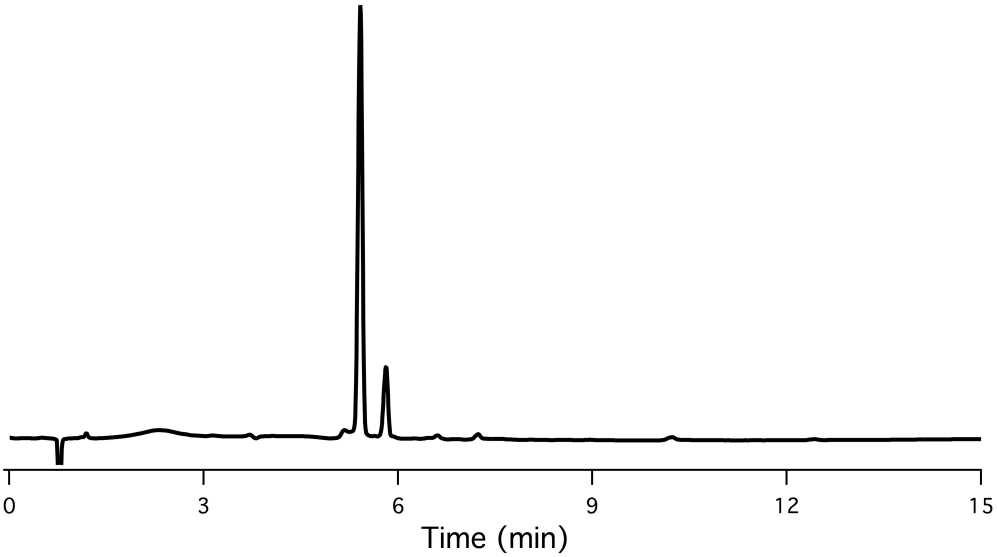

Figure S14. LC of $[Zn(CyHBET\text{-}OMe)]^{2-}$ detected at 280 nm showing both diastereomeric forms of this complex; m/z^{+} = 487.1 eluted with these peaks.

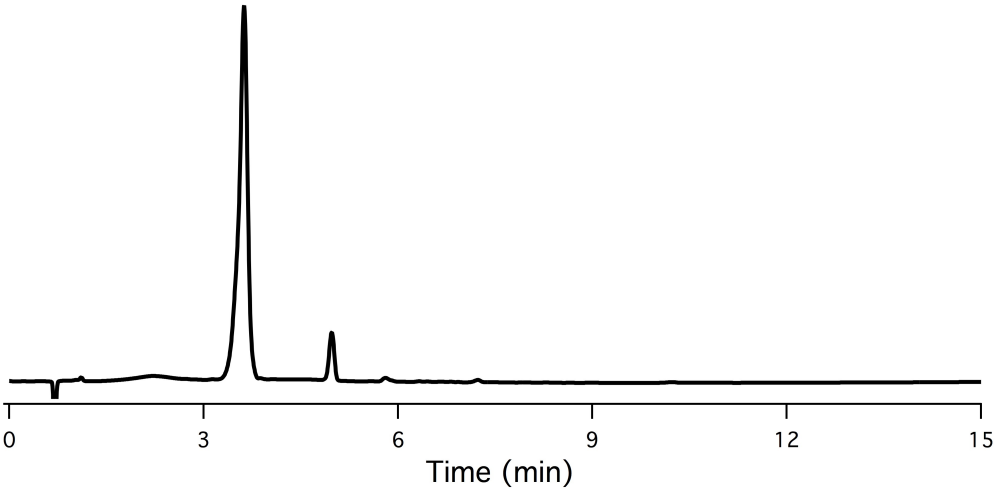

Figure S15. LC of $[Zn(CyHBET\text{-}NO_2)]^{2-}$ detected at 254 nm showing both diastereomeric forms of this complex; m/z^+ = 502.1 eluted with these peaks.

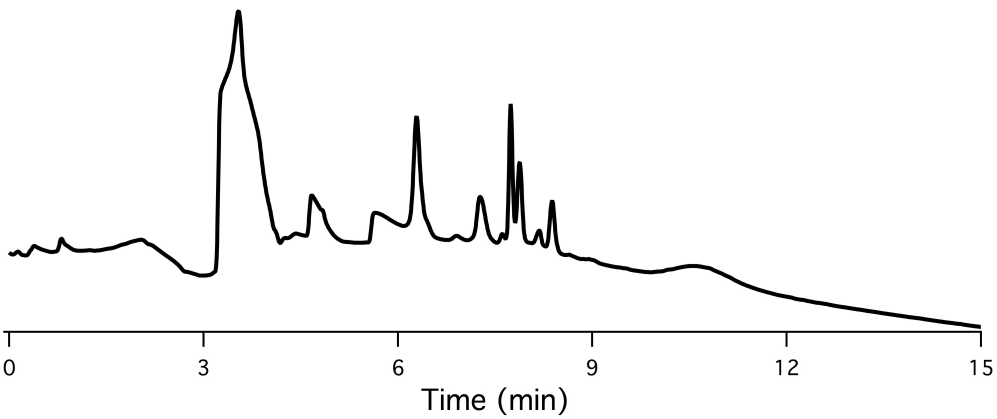

Figure S16. LC of crude reaction mixture of 1:1 HBET-OMe:MnF_3 at 220 nm detection.

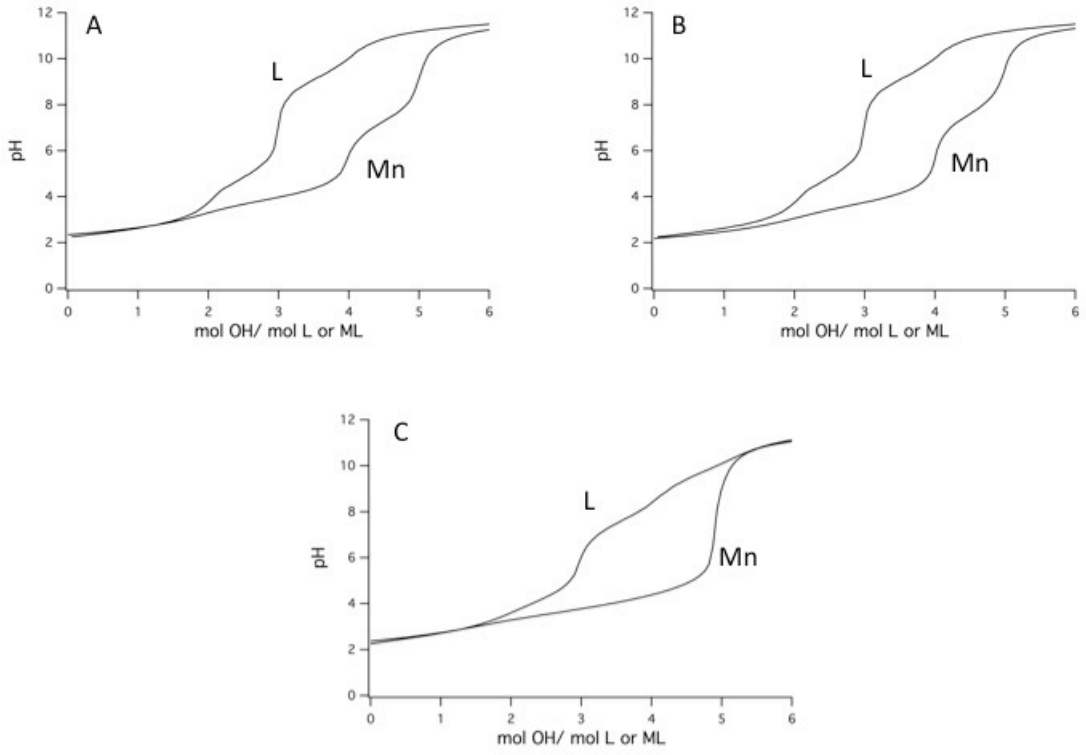

Figure S17. pH profiles of L and 1:1 Mn(II):L + 1 mol equiv. TFA. (A) HBET, (B) HBET-OMe, and (C) HBET-NO_2 (25 °C, *I* = 0.1 M NaCl).

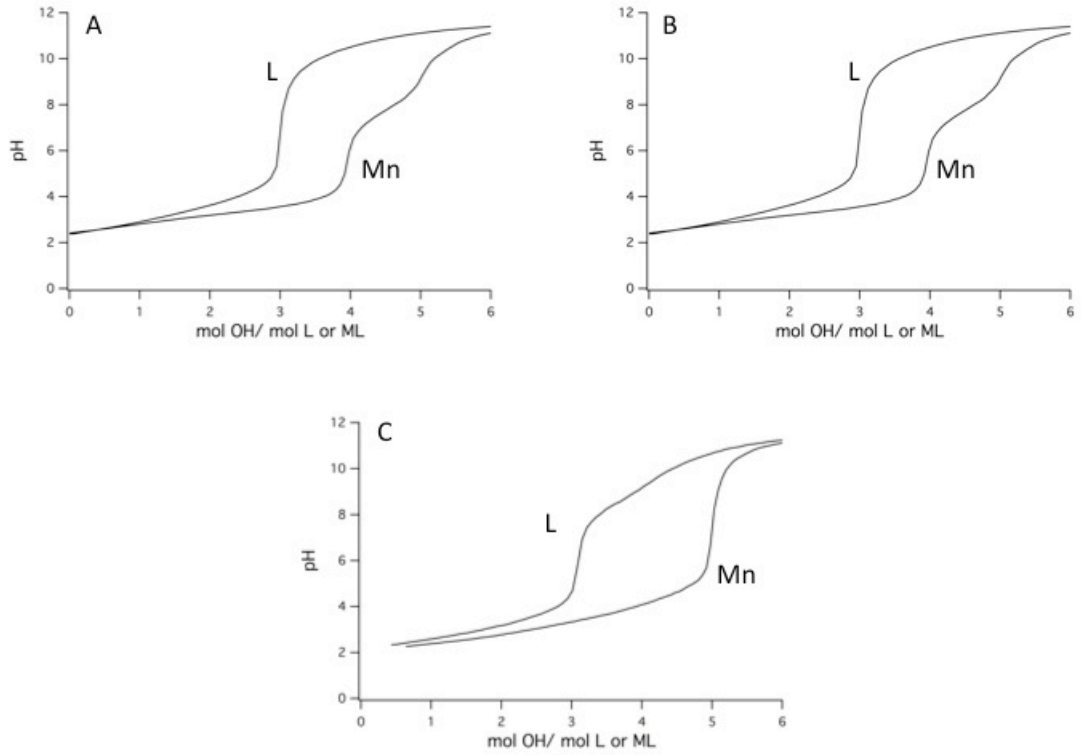

Figure S18. pH profiles of L and 1:1 Mn(II):L + 1 mol equiv. TFA. (A) CyHBET, (B) CyHBET-OMe, and (C) CyHBET-NO_2 (25 °C, *I* = 0.1 M NaCl).

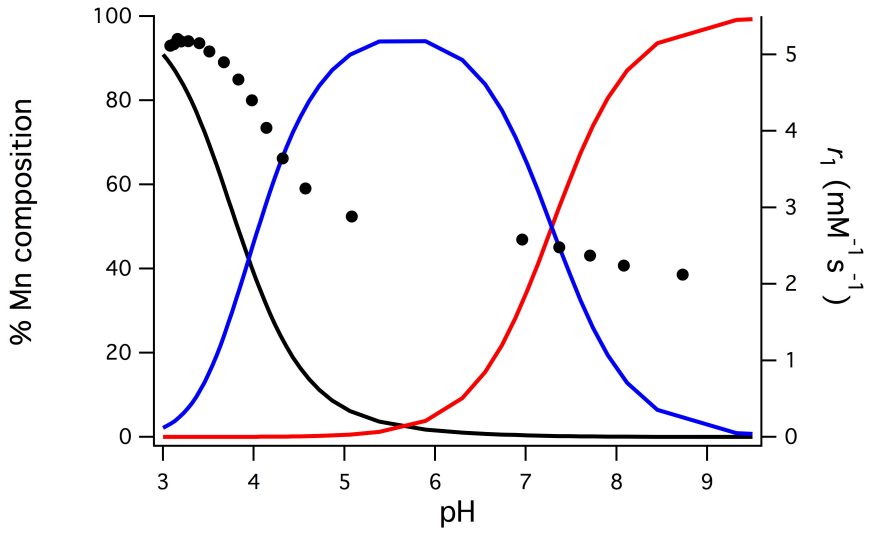

Figure S19. Distribution diagram for 1:1 Mn(II):HBET-OMe mixture. ML, HML and free Mn are depicted by red, blue and black traces, respectively ([Mn] = [L] =1 mM, 25 °C, *I* = 0.1 M NaCl); r_1 (37 °C, 1.4 T) is overlaid in black dots.

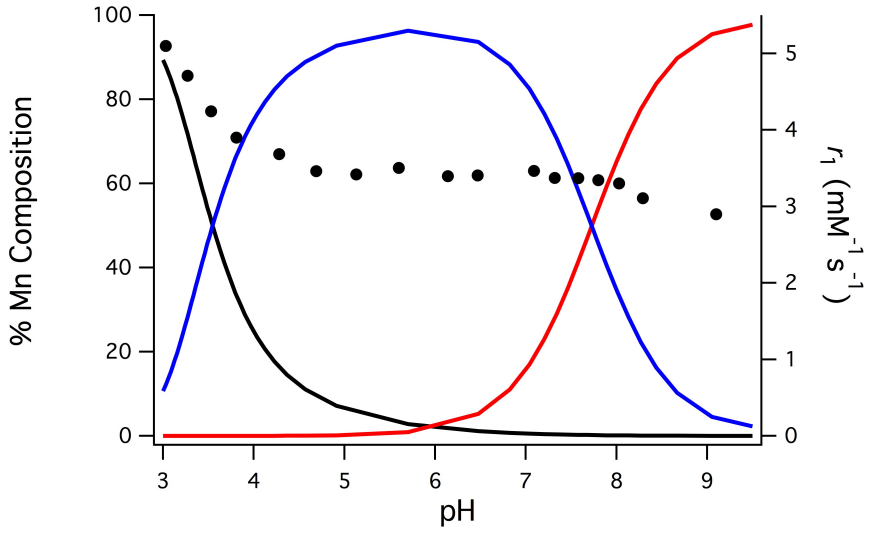

Figure S20. Distribution diagram for 1:1 Mn(II):CyHBET-OMe mixture. ML, HML and free Mn are depicted by red, blue and black traces, respectively ([Mn] = [L] =1 mM, 25 °C, *I* = 0.1 M NaCl); r_1 (37 °C, 1.4 T) is overlaid in black dots.

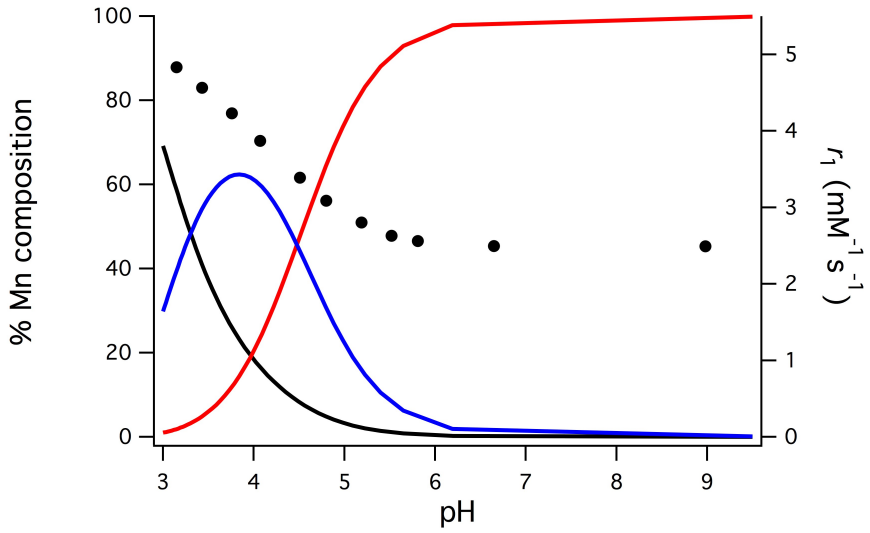

Figure S21. Distribution diagram for 1:1 Mn(II):CyHBET-NO_2 mixture. ML, HML and free Mn are depicted by red, blue and black traces, respectively ([Mn] = [L] =1 mM, 25 °C, I = 0.1 M NaCl); r_1 (37 °C, 1.4 T) is overlaid in black dots.

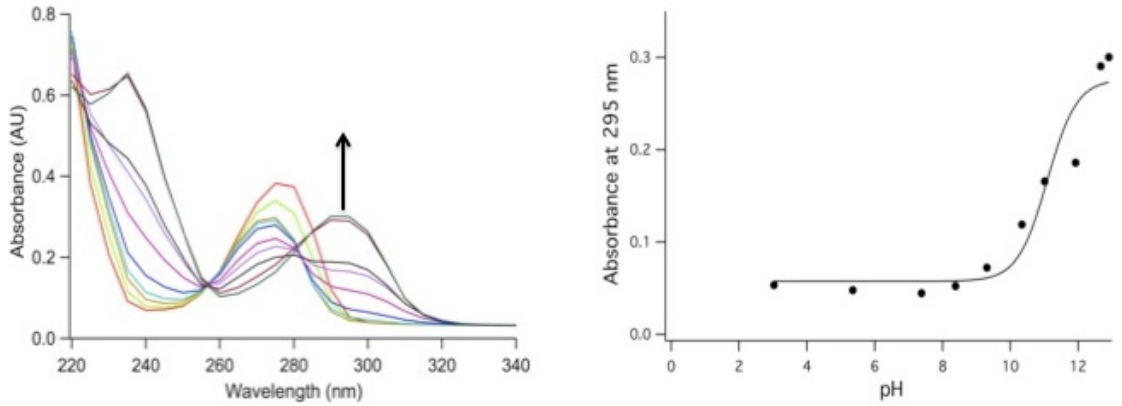

Figure S22. Left: UV-vis spectrum of HBET shown as a function of pH. Arrow indicates increase in absorbance at 295 nm with increasing pH. Right: Absorbance at 295 nm as a function of pH. Solid line represents the fit to the data.

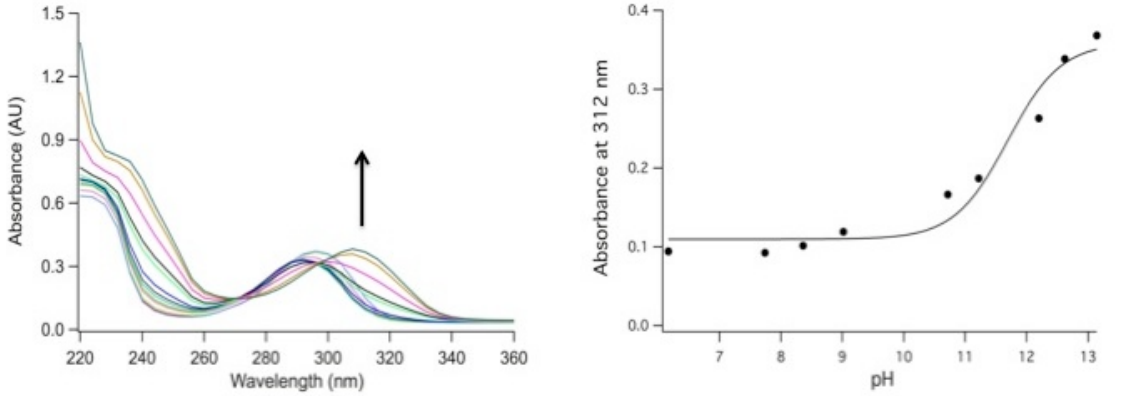

Figure S23. Left: UV-vis spectrum of HBET-OMe shown as a function of pH. Arrow indicates increase in absorbance at 312 nm with increasing pH. Right: Absorbance at 312 nm as a function of pH. Solid line represents the fit to the data.

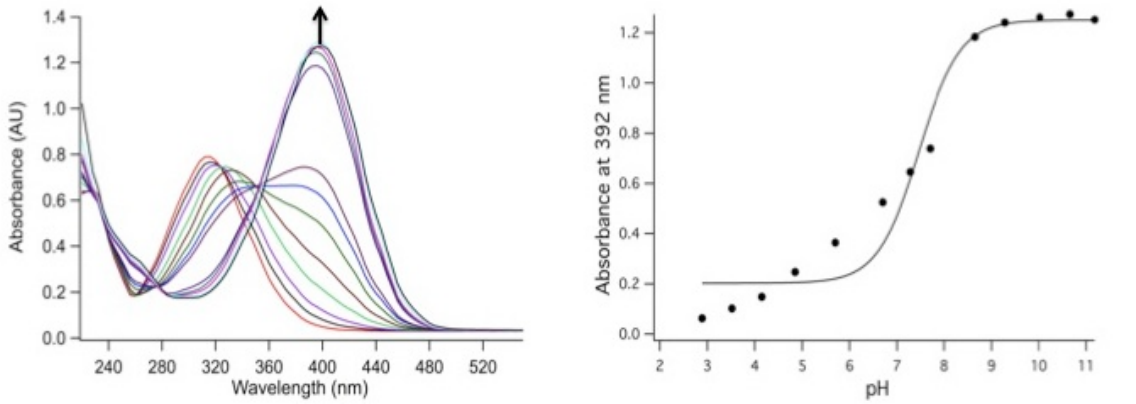

Figure S24. Left: UV-vis spectrum of HBET-NO_2 shown as a function of pH. Arrow indicates increase in absorbance at 410 nm with increasing pH. Right: Absorbance at 410 nm as a function of pH. Solid line represents the fit to the data.

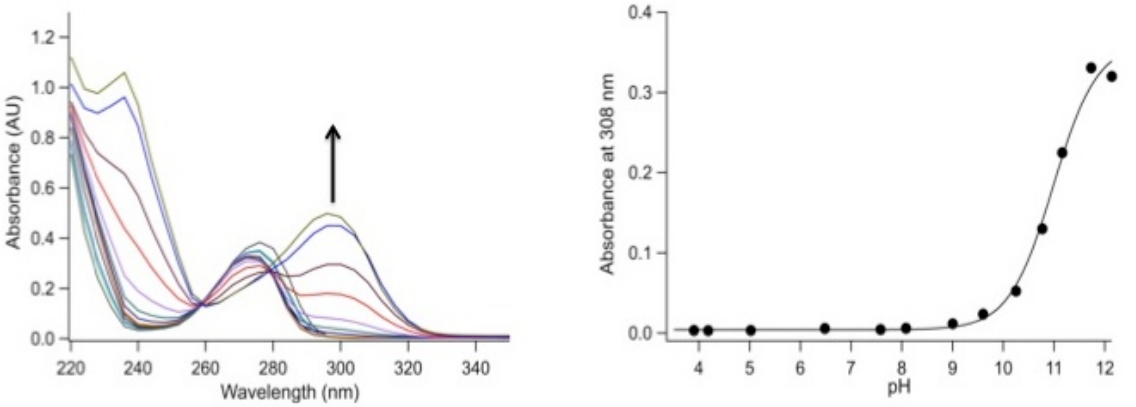

Figure S25. Left: UV-vis spectrum of CyHBET shown as a function of pH. Arrow indicates increase in absorbance at 308 nm with increasing pH. Right: Absorbance at 308 nm as a function of pH. Solid line represents the fit to the data.

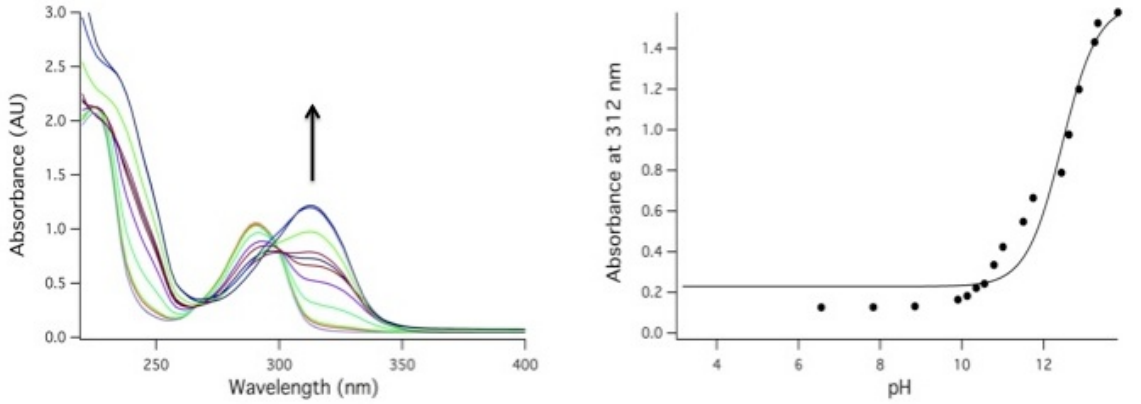

Figure S26. Left: UV-vis spectrum of CyHBET-OMe shown as a function of pH. Arrow indicates increase in absorbance at 312 nm with increasing pH. Right: Absorbance at 312 nm as a function of pH. Solid line represents the fit to the data.

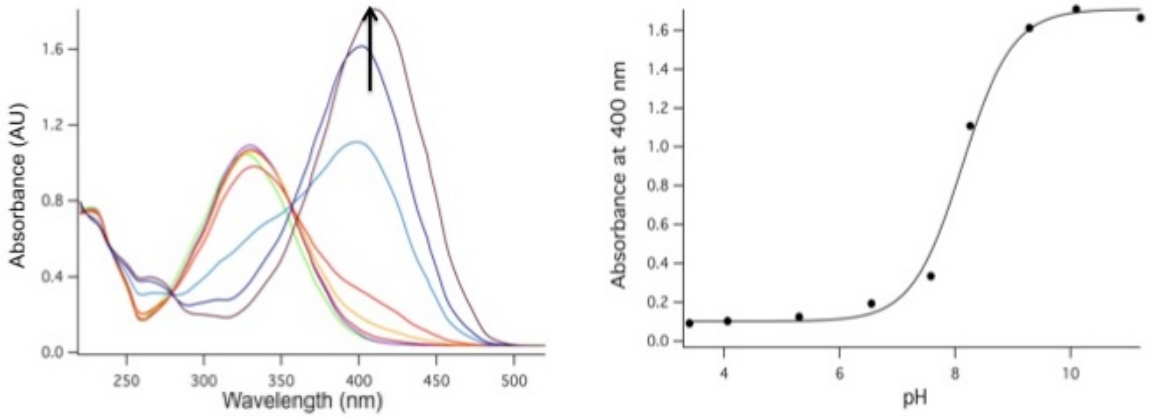

Figure S27. Left: UV-vis spectrum of CyHBET-NO_2 shown as a function of pH. Arrow indicates increase in absorbance at 400 nm with increasing pH. Right: Absorbance at 400 nm as a function of pH. Solid line represents the fit to the data.

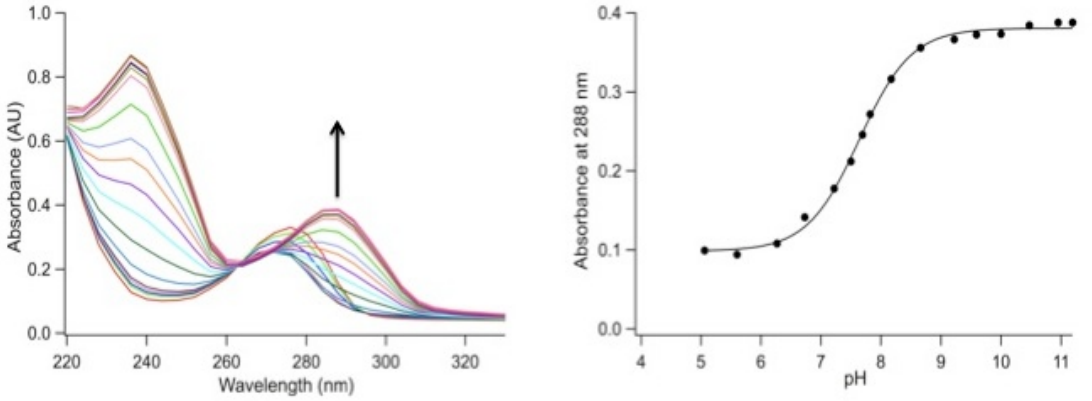

Figure S28. Left: UV-vis spectrum of $[Mn(HBET)]^{2-}$ shown as a function of pH. Arrow indicates increase in absorbance at 288 nm with increasing pH. Right: Absorbance at 288 nm as a function of pH. Solid line represents the fit to the data.

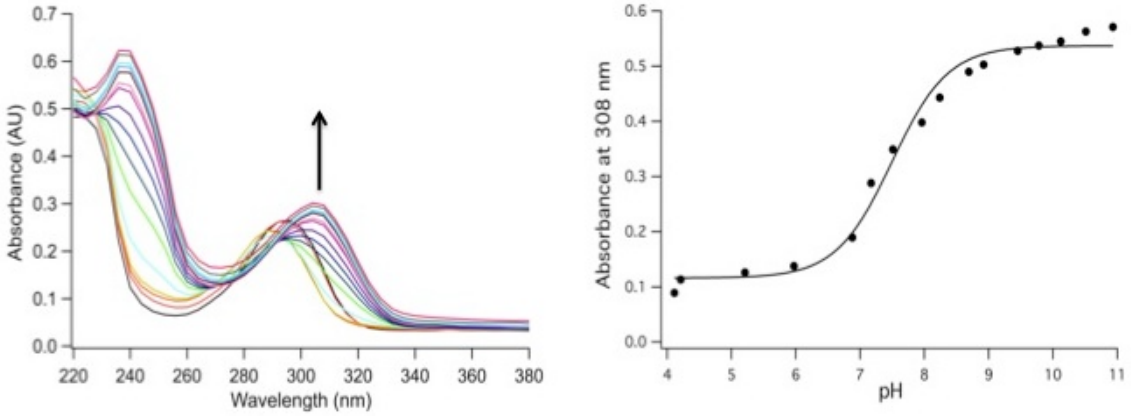

Figure S29. Left: UV-vis spectrum of $[Mn(HBET\text{-}OMe)]^{2-}$ shown as a function of pH. Arrow indicates increase in absorbance at 308 nm with increasing pH. Right: Absorbance at 308 nm as a function of pH. Solid line represents fit to the data.

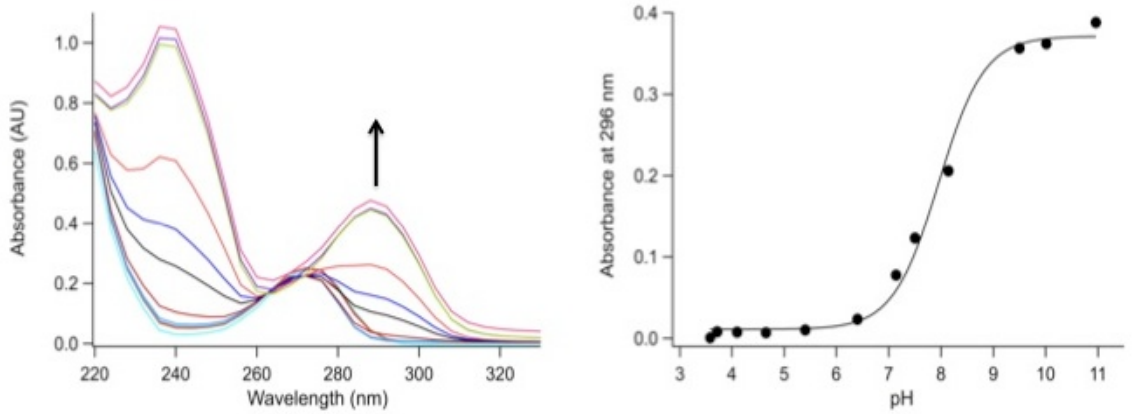

Figure S30. Left: UV-vis spectrum of $[Mn(CyHBET)]^{2-}$ shown as a function of pH. Arrow indicates increase in absorbance at 296 nm with increasing pH. Right: Absorbance at 296 nm as a function of pH. Solid line represents fit to the data.

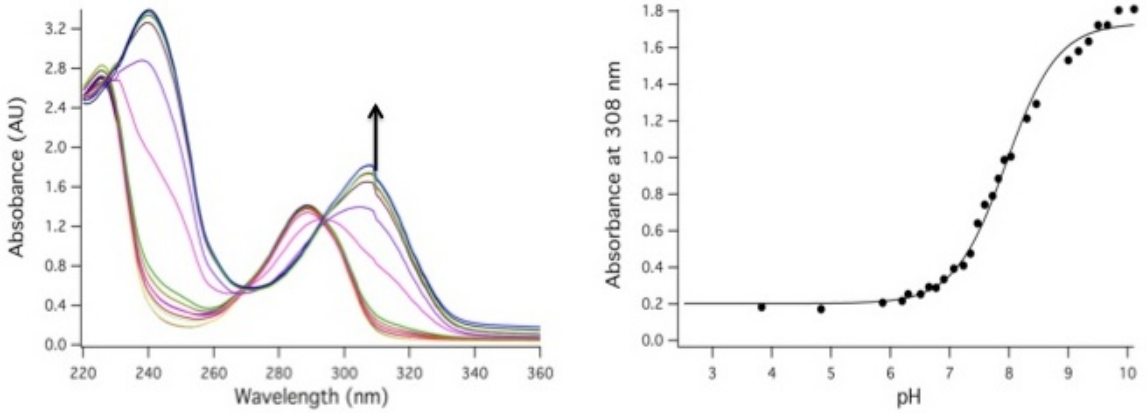

Figure S31. Left: UV-vis spectrum of $[Mn(CyHBET\text{-}OMe)]^{2-}$ shown as a function of pH. Arrow indicates increase in absorbance at 308 nm with increasing pH. Right: Absorbance at 296 nm as a function of pH. Solid line represents fit to the data.

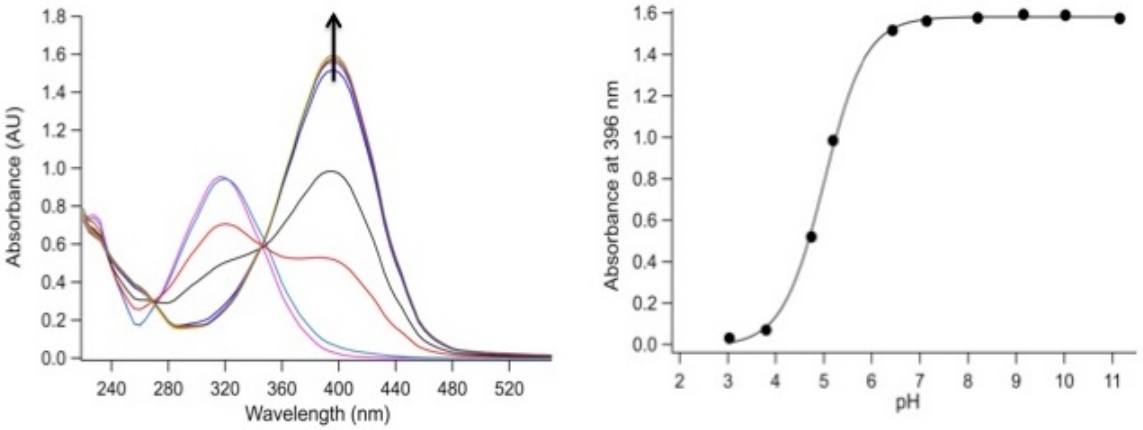

Figure S32. Left: UV-vis spectrum of $[Mn(CyHBET\text{-}NO_2)]^{2-}$ shown as a function of pH. Arrow indicates increase in absorbance at 396 nm with increasing pH. Right: Absorbance at 396 nm as a function of pH. Solid line represents fit to the data.

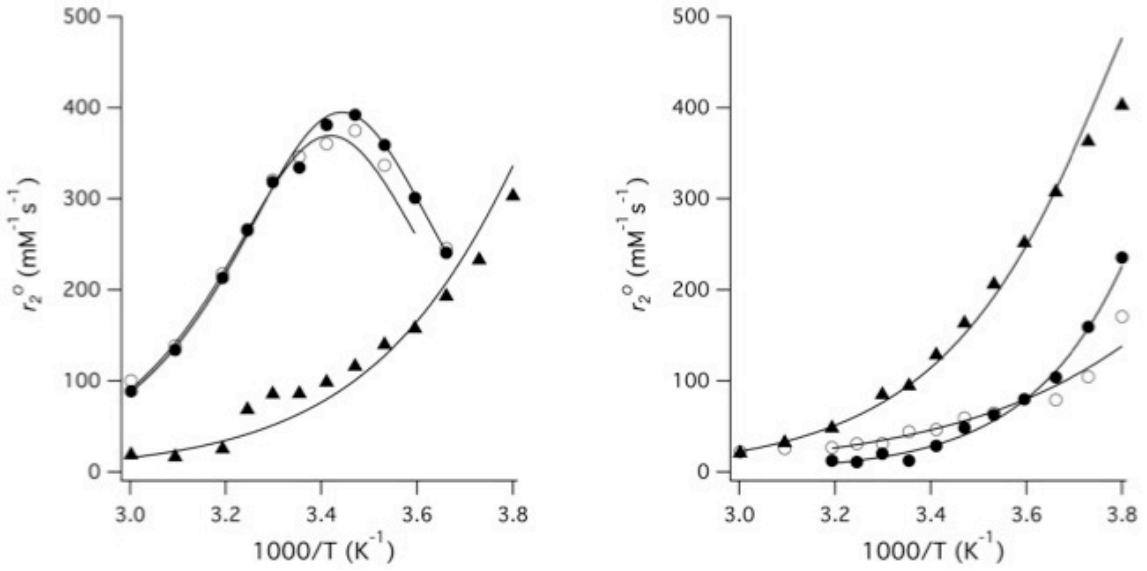

Figure S33. Plot of r_2^O as a function of temperature at pH 6 (left) and pH 9 (right) for $[Mn^{II}(CyHBET)]^{2-}$ (filled circles), $[Mn^{II}(CyHBET\text{-}OMe)]^{2-}$ (open circles), and $[Mn^{II}(CyHBET\text{-}NO_2)]^{2-}$ (triangles).

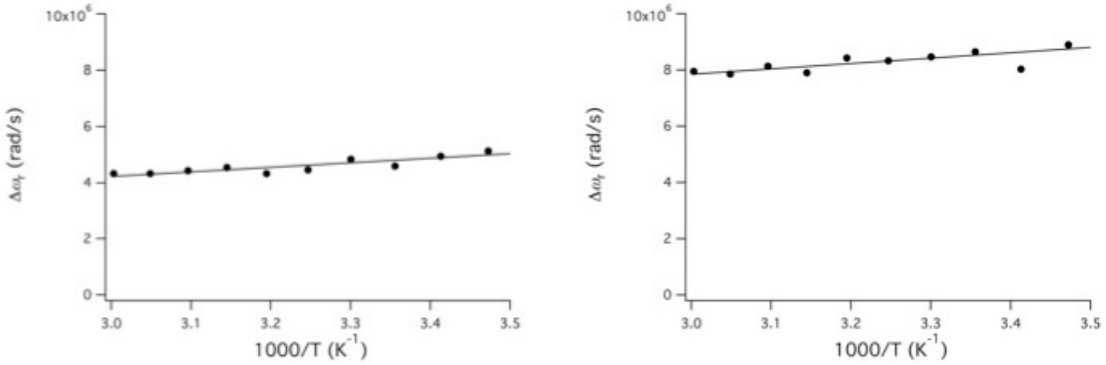

Figure S34. Reduced $H_2{}^{17}O$ chemical shift in the presence of $[Mn^{II}(HBET)]^{2-}$ (left) and $[Mn^{II}(HBET\text{-}OMe)]^{2-}$ (right) at pH 9.

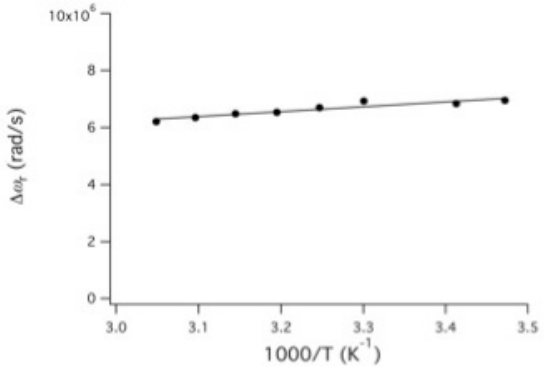

Figure S35. Reduced $H_2{}^{17}O$ chemical shift in the presence of $[Mn^{II}(CyHBET\text{-}NO_2)]^{2-}$ at pH 6.

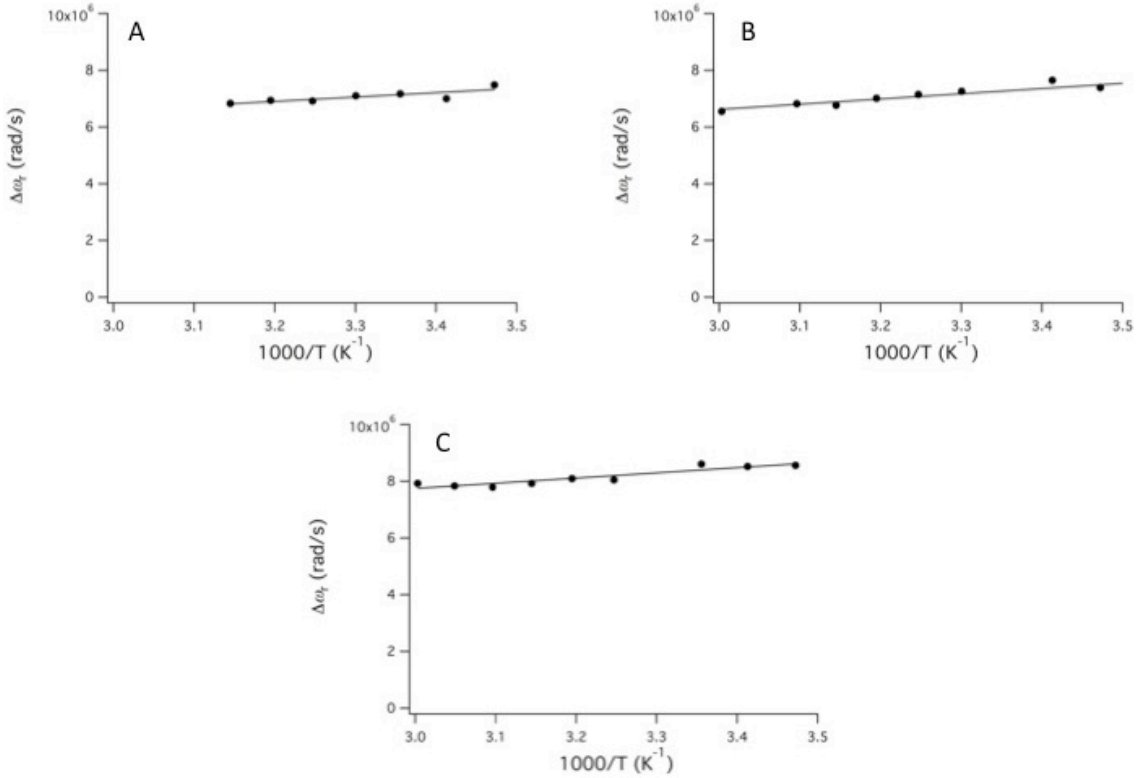

Figure S36. Reduced $H_2{}^{17}O$ chemical shift in the presence of (A) $[Mn^{II}(CyHBET)]^{2-}$, (B) $[Mn^{II}(CyHBET\text{-}OMe)]^{2-}$, and (C) $[Mn^{II}(CyHBET\text{-}NO_2)]^{2-}$ at pH 9.

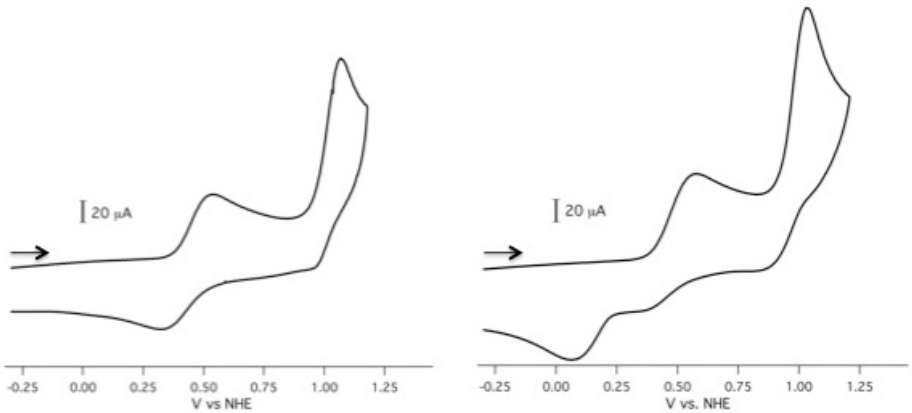

Figure S37. CV of $[Mn^{II/III}(HBET)]^{2-/1-}$ (left) and $[Mn^{II/III}(HBET\text{-}OMe)]^{2-/1-}$ (right) between -0.3 to 1.2 V. GC working electrode, Pt counter electrode, pH 7.4 with 0.5 M KNO_3 as supporting electrolyte, scan rate: 100 mV/s. Arrows indicate the position from which the scans were initiated.

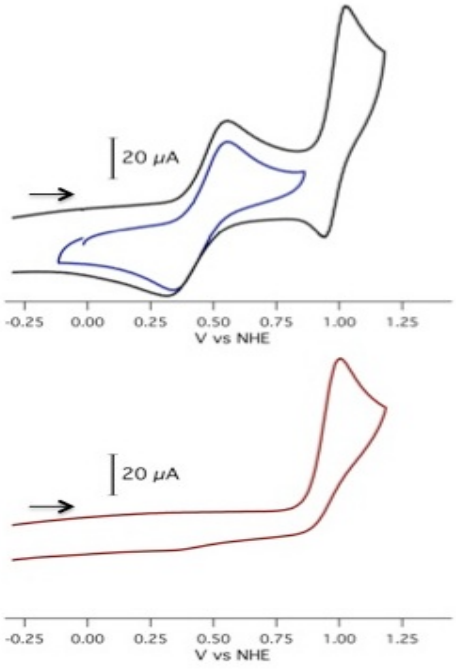

Figure S38. Top: CV of $[Mn^{II/III}(CyHBET)]^{2-/1-}$ between -0.3 to 0.7 V (blue) or -0.3 to 1.2V (black). Bottom: CV of $[Zn(CyHBET)]^{2}$. 5 mM complex, GC working electrode, Pt counter electrode, pH 7.4 w/ 0.5 M KNO_3 as supporting electrolyte, scan rate: 100 mV/s. Arrows indicate the position from which the scans were initiated.

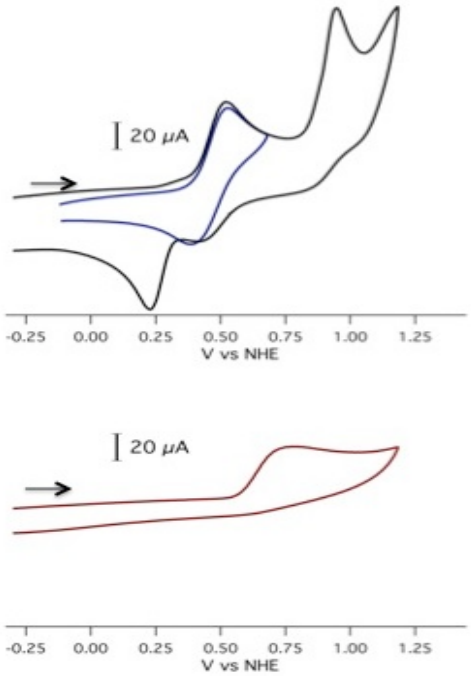

Figure S39. Top: CV of $[Mn^{II/III}(CyHBET\text{-}OMe)]^{2-/1-}$ between -0.3 to 0.7 V (blue) or -0.3 to 1.2 V (black). Bottom: CV of corresponding $[Zn(CyHBET\text{-}OMe)]^{2-}$ complex. 5 mM complex, GC working electrode, Pt counter electrode, pH 7.4 with 0.5 M KNO_3 as supporting electrolyte, scan rate: 100 mV/s. Arrows indicate the position from which the scans were initiated.

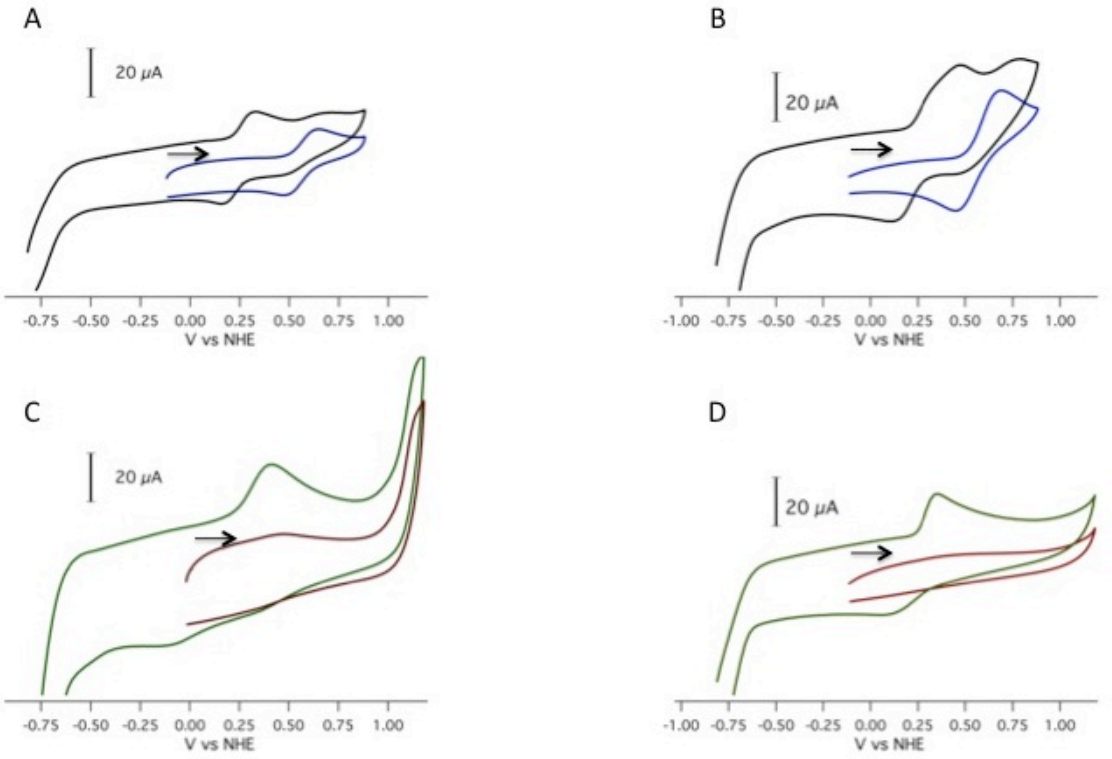

Figure S40. A: CV of $[Mn^{II/III}(HBET\text{-}NO_2)]^{2-/1-}$ scanning from -0.2 to 0.7 V (blue) or -0.3 to 1.2 V (black). B: CV of $[Mn^{II/III}(CyHBET\text{-}NO_2)]^{2-/1-}$ scanning from -0.2 to 0.7 V (blue) or 1.2 V (black). C: CV of $[Zn(HBET\text{-}NO_2)]^{2-}$. D: CV of $[Zn(CyHBET\text{-}NO_2)]^{2}$. 5 mM complex, GC working electrode, Pt counter electrode, pH 7.4 with 0.5 M KNO_3 as supporting electrolyte, scan rate: 100 mV/s. Arrows indicate the position from which the scans were initiated.

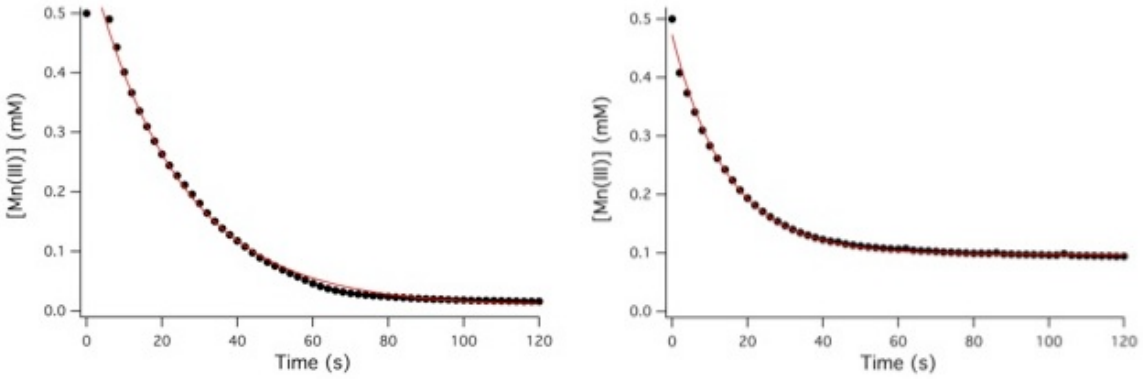

Figure S41. Conversion of 0.5 mM Mn(III) to Mn(II) in the presence of 10 mM cysteine in pH 7.4 Tris buffer. Left: $[Mn^{III}(HBET)]^-$. Right: $[Mn^{III}(CyHBET)]^-$.

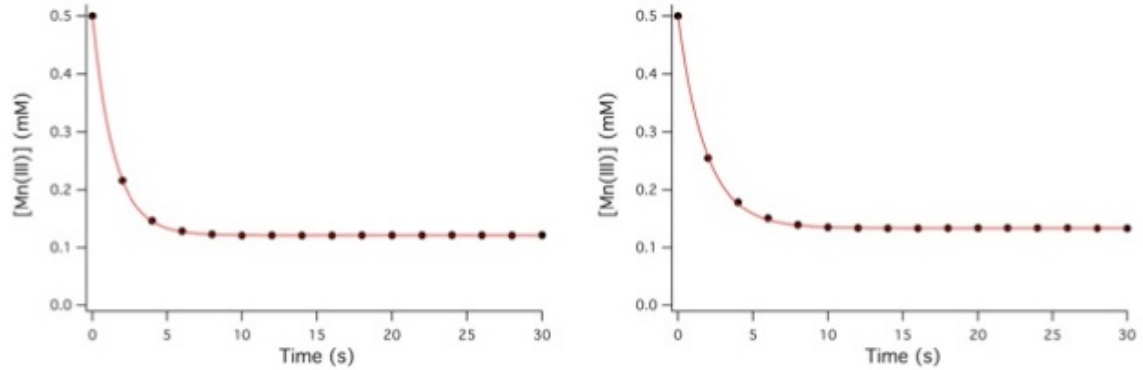

Figure S42. Conversion of 0.5 mM Mn(III) to Mn(II) in the presence of 10 mM cysteine in pH 7.4 Tris buffer. Left: $[Mn^{III}(HBET\text{-}NO_2)]^-$. Right: $[Mn^{III}(CyHBET\text{-}NO_2)]^-$.

Ligand	pK_a	Complex	pK_a
HBET	11.09	$[Mn(HBET)]^{2-}$	7.64
HBET-OMe	11.69	$[Mn(HBET\text{-}OMe)]^{2-}$	7.91
HBET-NO_2	7.46	$[Mn(HBET\text{-}NO_2)]^{2-}$	4.84
CyHBET	11.37	$[Mn(CyHBET)]^{2-}$	7.95
CyHBET-OMe	12.48	$[Mn(CyHBET\text{-}OMe)]^{2-}$	7.95
CyHBET-NO_2	8.12	$[Mn(CyHBET\text{-}NO_2)]^{2-}$	4.87

Table S1. Phenol pK_a Values Determined by UV-vis Spectroscopy.